Supporting Information for

An improved framework for efficiently modeling organic aerosol (OA) considering primary OA evaporation and secondary OA formation from VOCs, IVOCs, and SVOCs

Ling Huang[1], Zi'ang Wu[1], Hanqing Liu[1], Greg Yarwood[2,*], Dandan Huang[3], Gary Wilson[3], Hui Chen[1], Dongsheng Ji[4], Jun Tao[5], Zhiwei Han[6], Yangjun Wang[1], Hongli Wang[3], Cheng Huang[7], Li Li[1,*]

[1]School of Environmental and Chemical Engineering, Shanghai University, Shanghai, 200444, China
[2]Ramboll, Novato, California, 94945, USA
[3]State Environmental Protection Key Laboratory of Formation and Prevention of Urban Air Pollution Complex, Shanghai Academy of Environmental Sciences, Shanghai 200233, China
[4]Institute of Atmospheric Physics, Chinese Academy of Sciences, Beijing, 100029, China
[5]University of Chinese Academy of Sciences, Beijing, 100049, China
[6]Institute for Environmental and Climate Research, Jinan University, Guangzhou, 510632, China
[7]State Ecology and Environment Scientific Observation and Research Station for the Yangtze River Delta at Dianshan Lake, Shanghai Environmental Monitoring Center, Shanghai 200030, China

*Corresponding author:
Li Li, lily@shu.edu.cn; Phone: 86-21- 6613 7732
Greg Yarwood, gyarwood@ramboll.com; Phone: +1 415-899-0704

This file includes:

Section S1 SOA yields from evaporated POA in CMAQ AERO7

The SOA yields from the gas-phase portion of SVOCs in the AERO7 scheme were calculated using an offline conceptual model following our previous study (Huang et al., 2023). In the AERO7 scheme, POA emissions are initially allocated into five bins with volatilities ranging from 0.1 μg/m^3 to 10^3 μg/m^3 based on predefined fractions (refer to Table S1). The aging process of POA is represented by OH oxidation of gas-phase products across different volatility bins, with an OH rate constant (k_{OH}) of 4×10^{-11} cm^3/molecule/s, leading to the formation of products in different volatility bins. For example, VLVPO1 (C*=0.1 μg/m^3) reacts with OH following Eq. S1 (refer to CMAQ source codes for additional reactions):

VLVPO1 + OH = 0.4857 * VLVPO1 + 0.0062 * VSVPO1 + 0.0025 * VSVPO2 + 0.0026 * VSVPO3 + 0.0023 * VIVPO1 + 0.2944 * VLVOO1 + 0.2021 * VLVOO2 + 0.0019 * VSVOO2 + 0.0023 * VSVOO3	Eq. S1

where VLVPO1, VSVPO1, VSVPO2, VSVPO3, and VIVPO1 represent the gas-phase portion of SVOCs species; VLVOO1 (C*= 0.01 μg/m^3), VLVOO2 (0.1 μg/m^3), VSVOO2 (10 μg/m^3), and VSVOO3 (100 μg/m^3) are considered as SOA species.

At time 0, the fraction of POA emissions in each volatility bin is listed in Table S1. Eq. S2 illustrates how the total OA yields (gas-phase + particle phase) in each volatility bin (*i*) change with time (i.e. aging):

$\text{OA mass}\vert_t^i = \text{OA mass}\vert_{t-1}^i \times \left(f_{particle}^i + f_{gas}^i \cdot e^{-k_{OH} * [OH] * \Delta t}\right) + \sum_k^{10}[\text{OA mass}\vert_{t-1}^k \times f_{gas}^k \cdot (1 - e^{-k_{OH} * [OH] * \Delta t}) \times \alpha_k^i]$	Eq. S2

The first half on the right hand side of Eq. S2 represents the remaining OA mass within the current volatility bin (*i*) from the preceding time step (t-1), accounting for the nonreactive particle-phase fraction ($f_{particle}^i$) and the residual gas-phase fraction subsequent to OH oxidation ($f_{gas}^i \cdot e^{-k_{OH} * [OH] * \Delta t}$). The second half represents the gained OA mass through oxidation from a total of 10 different bins, with α_k^i denoting the mass yield coefficient from bin k to bin i (i.e., numerical values in Eq. S1) and $f_{gas}^k \cdot (1 - e^{-k_{OH} * [OH] * \Delta t})$ representing the reacted gas-phase fraction. The gas- (f_{gas}^i) and particle-phase fractions ($f_{particle}^i$) for each volatility bin are simply calculated based on the Pankow's partitioning theory (Eq.3).

Several assumptions were made during the calculation. Firstly, an annual OH concentration of 1.5 ×

10^6 molecules/cm^3 was used. Secondly, the aforementioned calculation was performed every 0.2 hours until an integrated OH exposure of 10^{10} molecules/cm^3·s (equal to a 2-hour exposure time) was reached to represent typical amount of aging. Subsequently, the total increased mass in the particle-phase from all volatility bins (ΔOA_p) was determined, and the mass yields in g/g were calculated by dividing the total reacted mass:

$\text{OA mass yield (g/g)} = (\Delta OA_p\|_{t=0}^{t=2hr})/\Delta\, precursor\ reacted$	
$\Delta\, OA_p = (\sum_k^{10} OA\ yield\|_{t=2hr}^{k} \cdot f_{particle}^{k} - \sum_k^{10} OA\ yield\|_{t=0}^{k} \cdot f_{particle}^{k})/\Delta\, precurosr\ reac$	Eq. S3
$\Delta\, precursor\ reacted = \sum_{t=0}^{t=2hr} [\text{OA yield}\|_{t-1}^{k} \times f_{gas}^{k} \cdot (1 - e^{-k_{OH} * [OH] * \Delta t})]$	Eq. S4

For example, with a C_{OA} = 10 μg/m^3, the POA concentration in the particle-phase was 0.167 μg/m^3 at t = 0. With 2 hours of OH oxidation, the total OA concentration in the particle-phase was 0.403 μg/m^3, indicating a mass increase by a factor of 2.4. The amount of reacted precursors was calculated to be 0.346 μg/m^3; thus the OA mass yield under C_{OA}=10μg/m^3 was determined to be 0.682 g/g.

These calculations were repeated for different ambient OA concentrations (C_{OA} = 0.1 μg/m^3 to 100 μg/m^3) and the corresponding OA mass yields were obtained. Subsequently, these results were used to determine the stoichiometric coefficients ($\alpha_{1,SVOCs}$, $\alpha_{2,SVOCs}$, and $\alpha_{3,SVOCs}$) in SOAP3 that yielded the best fit with the AERO7 results (Figure 2b).

It is important to highlight that the total increase in particle-phase mass in AERO7 includes contributions from all ten bins. Among these, five bins (VLVPO1, VSVPO1, VSVPO2, VSVPO3, and VIVPO1) are classified as POA, while the remaining five bins (VLVOO1, VLVOO2, VSVOO1, VSVOO2, and VSVOO3) are considered SOA generated from SVOCs. In SOAP3, however, POA is treated as an inert species, with all the increased mass attributed to SOA formation from SVOCs. Consequently, SOA yields from SVOCs are slightly higher in SOAP3 compared to AERO7, as illustrated in Figure 7 and Figure S4 ~ S5.

Section S2 Updates of SOA formation in CAMx SOAP3

Simulations based on CMAQ AERO7 indicate substantial SOA contributions from heterogeneous uptake of glyoxal (GLY) and methylglyoxal (MGLY) onto particles during the daytime, as well as the formation of organic nitrates from monoterpene + NO_3 during the nighttime. However, the default CAMx version, does not account for the former pathway and the latter pathway was found to be significantly underestimated. In response, adjustments were made in CAMx SOAP3 to align with the AERO7 results.

(1) Updating yields of organic nitrates

In CMAQ AERO7, the reaction of monoterpene (TERP) with NO_3 produces an intermediate product, $TERPNRO_2$, which subsequently reacts with NO, HO_2, NO_3, and RO_2 to form $MTNO_3$ (C^*=12 μg/m^3):

TERP + NO_3 -> $TERPNO_2$	Eq. S5
$TERPNO_2$ + NO -> 0.688 $MTNO_3$ + other products	Eq. S6
$TERPNO_2$ + HO_2 -> 1.0 $MTNO_3$	Eq. S7
$TERPNO_2$ + NO_3 -> 0.422 $MTNO_3$ + other products	Eq. S8
$TERPNO_2$ + RO_2 -> 0.711 $MTNO_3$ + other products	Eq. S9

The resulting particle-phase of $MTNO_3$ undergoes aerosol hydrolysis to produce a non-volatile product (MTHYD), at a rate constant of 9.49×10^{-6} s^{-1}. For each pathway (Eq. S6-S9), we calculated the total SOA yields, including $MTNO_3$ and MTHYD, at different OA concentrations, assuming a hydrolysis time of 9 hours. Similar to how we fit the SOA yields for other precursors, we obtained the SOAP3 parameters at different OA values that yields best match with the AERO7 results.

(2) Heterogeneous uptake of GLY and MGLY on aerosol surface

The pseudo-first order rate coefficient for GLY/MGLY (k') was parameterized as Eq. S10 (Walker et al., 2022):

$k'_{GLY/MGLY} = \left(\frac{r}{D_g} + \frac{4}{\gamma_{GLY/MGLY} c_g}\right)^{-1} A$	Eq. S10

where r is the aerosol particle effective radius, D_g is the gas-phase diffusion coefficient for GLY/MGLY, γ is the uptake coefficient, c_g is the mean molecular speed, and A is the aerosol surface area per unit volume. We added this pathway in CAMx with γ values adopted from Walker et al. (2022; 0.001 for GLY) and 9% of GLY for MGLY (from AERO7) while the remaining parameters were calculated in-line by CAMx.

Table S1 Volatility distribution factors used to allocate POA emissions to the five bins for AERO7 scheme in CMAQ

Volatility bin for POA	VLVPO1	VSVPO1	VSVPO2	VSVPO3	VIVPO1
C^* ($\mu g/m^3$, T=298K)	0.1	1	10	100	1000
Emission fraction	0.09	0.09	0.14	0.18	0.5
ΔH_{vap} (kJ/mol)	89	85	81	77	73

Table S2 SOA parameters for CAMx SOAP3

SOA precursors	CG or SOA species	C^* @ 300 K ($\mu g/m^3$)	ΔH_{vap} (kJ/mol)	MW (g/mol)
Anthropogenic precursors (benzene/toluene/xylene/ IVOCs/SVOCs)	CG1	14	80	150
	CG2	0.31	85	150
	SOPA	0	/	220
BVOCs (isoprene/monoterpene/ sesquiterpenes)	CG3	26	80	180
	CG4	0.45	85	180
	SOPB	0	/	220

Table S3 SOA mass-yield coefficients used in the CMAQ AERO7 scheme (unit:g/g)

NO*x* conditions	Precursor	SOA yields for volatility bin with C^* (μg/m^3, T=298K) of											SOA mass yields at C_{OA} = 10 μg/m^3
		1	10	100	1000	0.01	116.01	0.617	24.984	0.1	10000	0	
High NO*x*	Benzene	0.078	0	0.793		0							0.140
	Toluene	0.031	0.094	0.081		0							0.081
	Xylene	0.025	0.037	0.089		0							0.049
	Isoprene						0.232	0.029					0.044
	Sesquiterpenes								1.537				0.408
	Monoterpenes	0.032	0.103	0.143	0.285	0.04				0.032	0.16		0.161
	IVOCs											1.0	1.0
Low NO*x*	Benzene	0	0	0		0.370							0.370
	Toluene	0	0	0		0.301							0.301
	Xylene	0	0	0		0.360							0.360
	Isoprene						0.232	0.029					0.044
	Sesquiterpenes								1.537				0.408
	Monoterpenes	0.032	0.103	0.143	0.285	0.040				0.032	0.16		0.161
	IVOCs											1.0	1.0

Table S4 List of different scenarios conducted in this study

Scenario	VOCs emissions	IVOCs emissions	SVOCs emissions
Base	✓	✓	✓
No_SVOCs	✓	✓	
No_S/IVOCs	✓		

S/IVOCs emission inventory are developed by Wu et al. (2021)

Table S5 Location of monitoring sites and $(OC/EC)_{pri}$ value for each site

Month	Site	Abbreviation	Longitude (°)	Latitude (°)	$(OC/EC)_{pri}$
Jul.	Beijing	BJ	116.4	39.8	0.7
	Tianjin	TJ	117.2	39.0	1.1
	Qinhuangdao	QHD	119.6	39.9	0.7
	Zhangjiakou	ZJK	114.8	40.8	1.1
	Taiyuan	TY	112.5	37.8	1.4
	Nanjing	NJ	118.7	32.0	0.4
	Changzhou	JS_CZ	119.9	31.7	0.3
	Dianshan Lake	DSL	120.9	31.0	1.0
	Guangzhou	GZ	113.2	23.1	0.8
	Dongguan	DG	113.7	23.0	1.1
Nov.	Beijing	BJ	116.4	39.8	1.2
	Tianjin	TJ	117.2	39.0	1.3
	Cangzhou	HB_CZ	116.7	38.2	1.0
	Changzhou	JS_CZ	119.9	31.7	1.1
	Shanghai	SH	121.5	31.2	1.4
	Suzhou	SZ	120.6	31.3	0.4

Table S6 Evaluation results of $PM_{2.5}$ simulation by SOAP3 in selected areas

Month	Region	R	MB (μg/m^3)	RMSE	NMB (%)	NME (%)
July	BTH	0.31	1.7	23.3	4%	43%
	YRD	0.45	4.0	24.2	16%	68%
	PRD	0.38	-8.5	12.0	-48%	57%
	SCB	0.15	22.9	34.2	106%	125%
	FWP	0.48	-2.1	16.4	-6%	35%
	Northeast	0.48	1.0	13.6	5%	48%
November	BTH	0.60	-23.1	51.8	-28%	40%
	YRD	0.76	8.8	32.8	17%	45%
	PRD	0.30	-0.6	18.4	-2%	38%
	SCB	0.61	25.0	38.9	58%	70%
	FWP	0.48	-21.9	43.7	-29%	41%
	Northeast	0.56	-5.2	24.4	-13%	41%

Table S7 Domain averaged concentration for each OA component by selected region (μg/m^3)

Month	Region	Models	POA	SOA	ASOA	BSOA	IVOC-SOA	SVOC-SOA	OA	SOA/OA
Jul.	BTH	SOAP2	3.0	4.2	1.4	1.7	1.1	/	7.3	58.3%
		AERO7	1.9	9.9	1.5	4.4	3.6	0.3	11.8	83.8%
		SOAP3	2.2	9.1	1.0	4.0	3.6	0.6	11.3	80.8%
	YRD	SOAP2	2.3	5.6	1.0	4.0	0.6	/	7.9	70.8%
		AERO7	1.6	10.9	0.8	8.5	1.5	0.1	12.5	87.3%
		SOAP3	1.6	9.9	0.6	7.1	1.9	0.3	11.6	85.9%
	PRD	SOAP2	1.3	4.5	0.6	3.6	0.3	/	5.8	76.9%
		AERO7	1.0	8.5	0.5	7.2	0.7	0.1	9.5	90.0%
		SOAP3	1.0	6.5	0.3	5.1	0.9	0.2	7.5	86.9%
	SCB	SOAP2	2.3	4.4	0.6	3.4	0.4	/	6.7	65.6%
		AERO7	1.2	5.7	0.4	4.6	0.7	0.1	6.9	83.2%
		SOAP3	1.8	8.2	0.6	6.2	1.2	0.4	10.1	82.0%
	FWP	SOAP2	2.4	4.5	0.9	2.4	1.2	/	6.9	65.1%
		AERO7	1.4	9.3	1.0	4.8	3.2	0.2	10.7	86.7%
		SOAP3	1.8	9.8	0.8	4.9	3.6	0.6	11.7	84.2%

Month	Region	Models	POA	SOA	ASOA	BSOA	IVOC-SOA	SVOC-SOA	OA	SOA/OA
Nov.	BTH	SOAP2	9.8	1.4	0.7	0.1	0.6	/	11.2	12.4%
		AERO7	10.9	5.6	1.1	1.4	2.8	0.2	16.6	34.0%
		SOAP3	10.6	4.0	0.8	0.8	1.8	0.5	14.5	27.2%
	YRD	SOAP2	6.7	3.2	1.6	0.7	1.0	/	9.9	32.3%
		AERO7	7.7	10.8	2.3	3.5	4.7	0.3	18.5	58.5%
		SOAP3	6.4	8.4	1.5	2.5	3.6	0.9	14.8	56.8%
	PRD	SOAP2	3.0	4.9	1.7	2.4	0.8	/	7.9	62.1%
		AERO7	2.9	13.0	1.9	7.7	3.1	0.2	15.9	81.9%
		SOAP3	2.8	11.2	1.3	5.9	3.2	0.8	14.0	80.2%
	SCB	SOAP2	3.4	2.1	1.0	0.6	0.5	/	5.5	38.4%
		AERO7	3.3	4.6	0.9	1.8	1.7	0.1	7.9	58.8%
		SOAP3	3.4	5.4	1.1	1.8	1.9	0.6	8.8	61.0%
	FWP	SOAP2	6.6	1.7	0.8	0.2	0.8	/	8.3	20.8%
		AERO7	6.8	6.3	1.1	1.3	3.6	0.2	13.1	47.8%
		SOAP3	7.1	5.1	1.0	0.9	2.6	0.7	12.2	41.8%

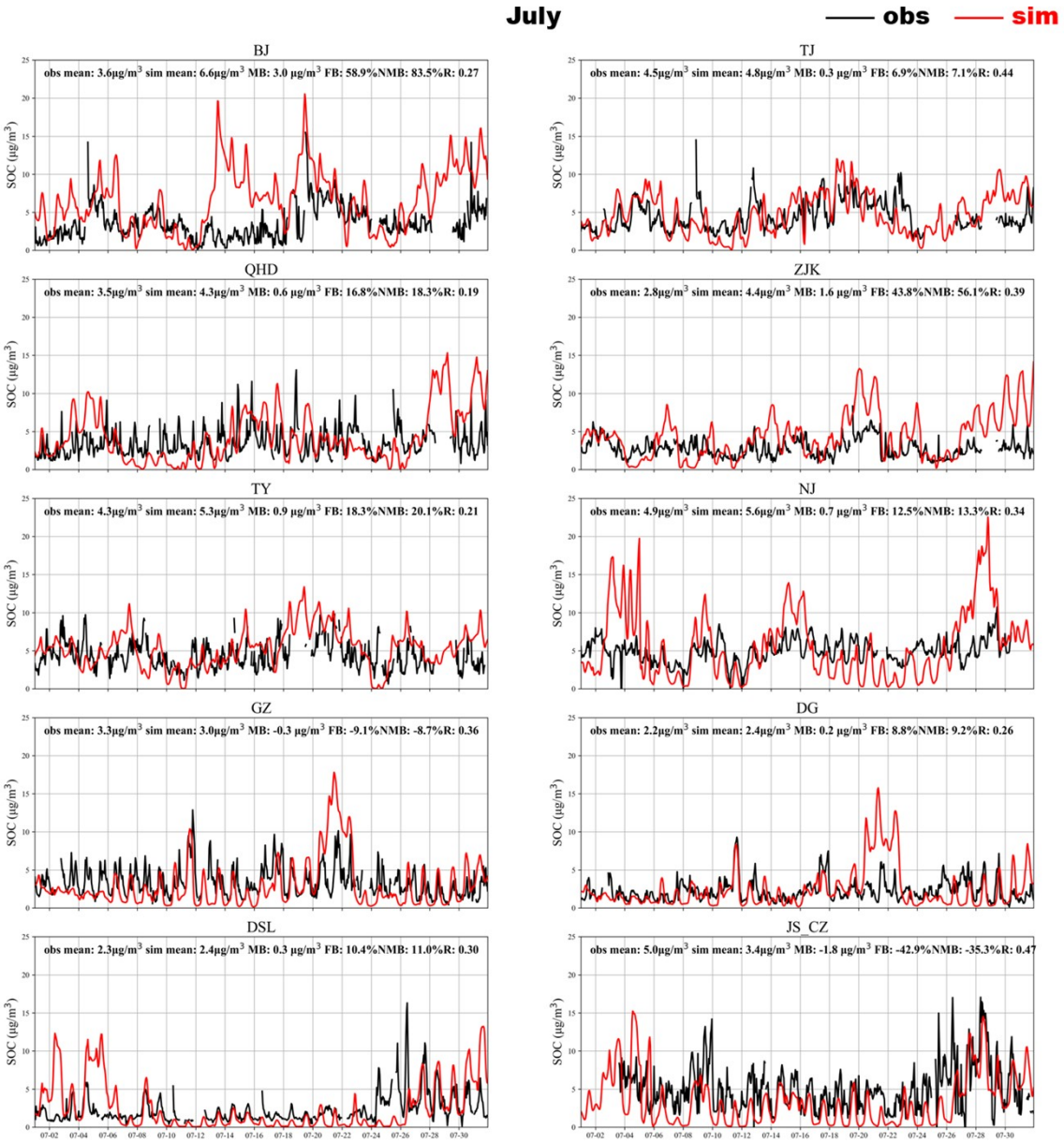

Figure S1 Time series of hourly observed and simulated SOC concentration for SOAP3 at 10 OC/EC observation sites in July 2018

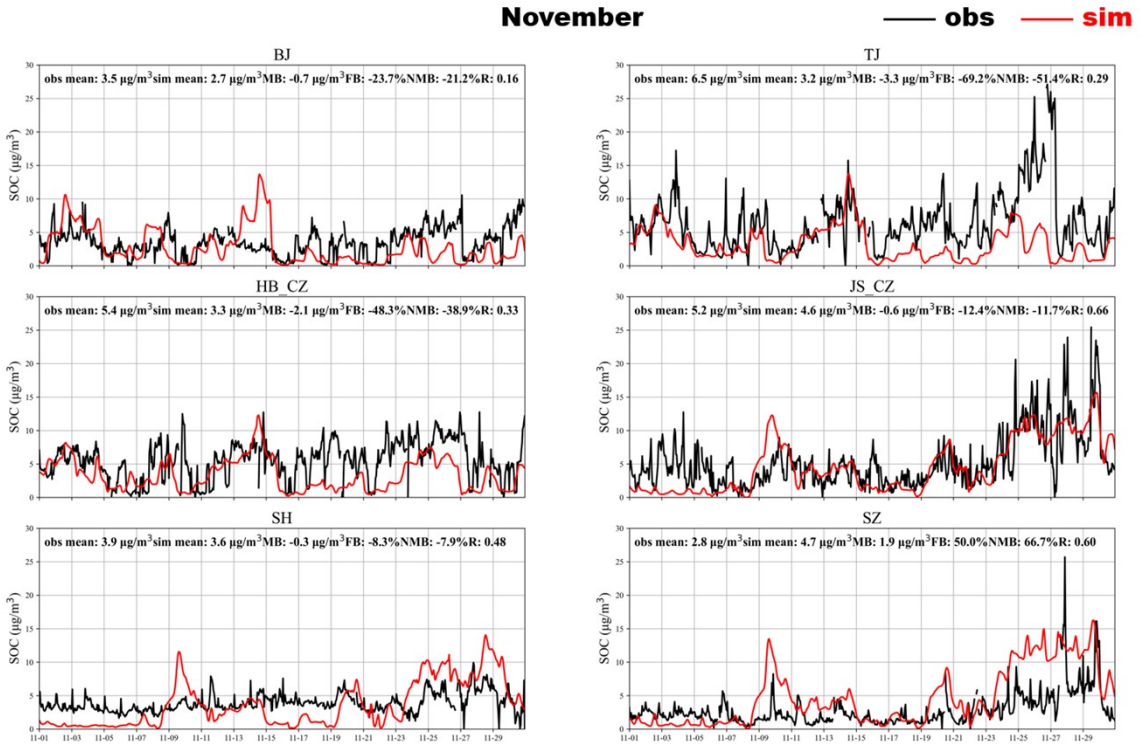

Figure S2 Time series of hourly observed and simulated SOC concentration for SOAP3 at 6 OC/EC observation sites in November 2018

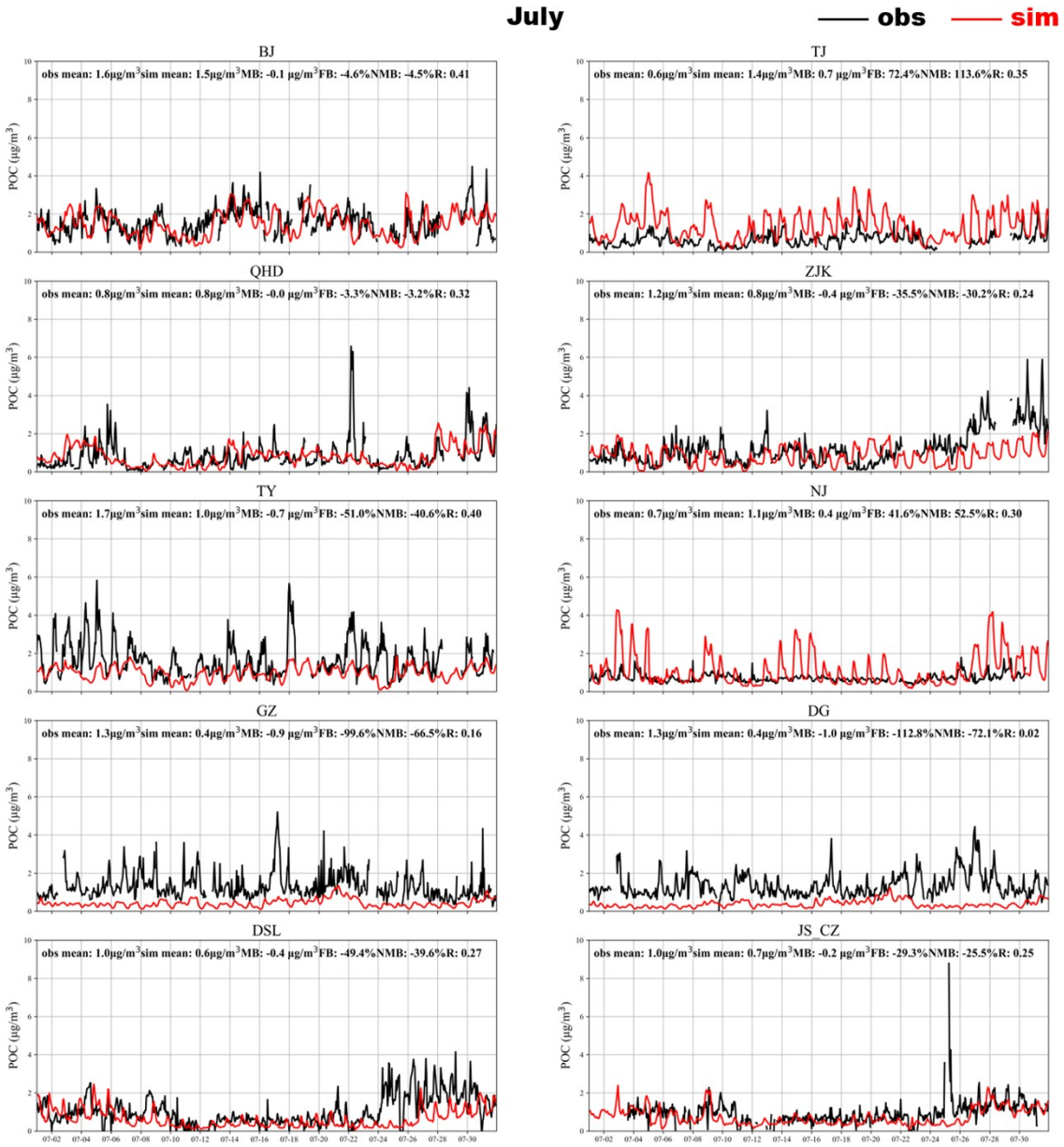

Figure S3 Time series of hourly observed and simulated POC concentration for SOAP3 at 10 OC/EC observation sites in July 2018

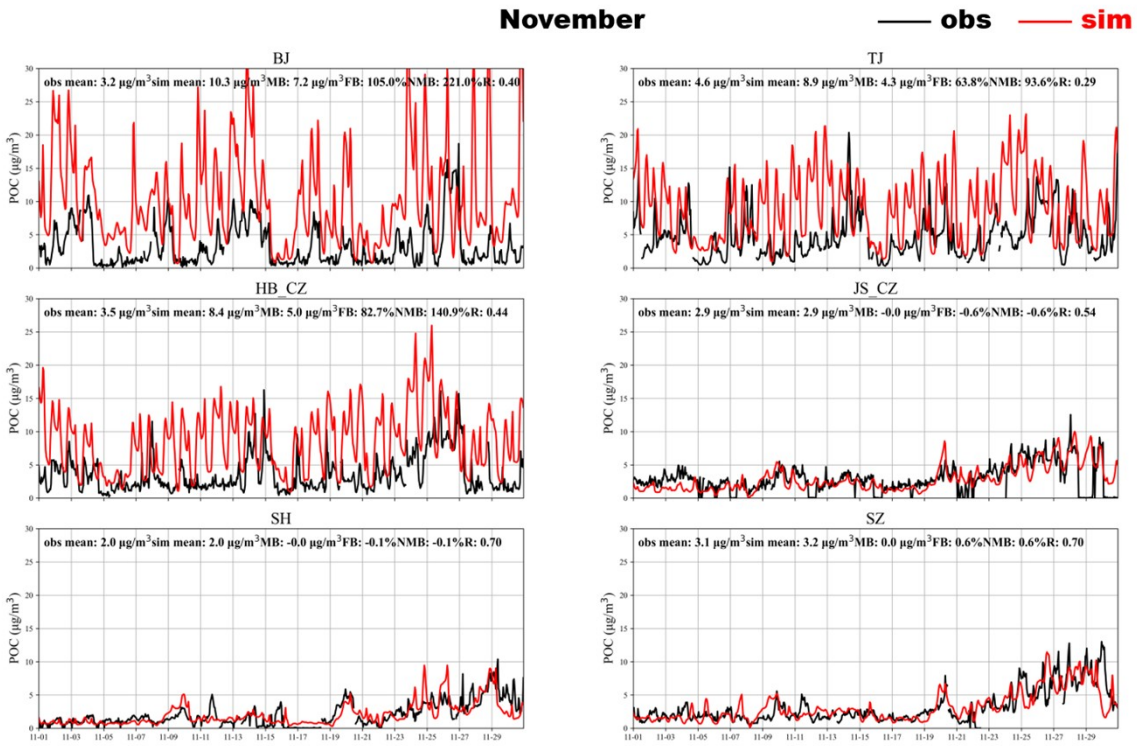

Figure S4 Time series of hourly observed and simulated POC concentration for SOAP3 at 6 OC/EC observation sites in November 2018

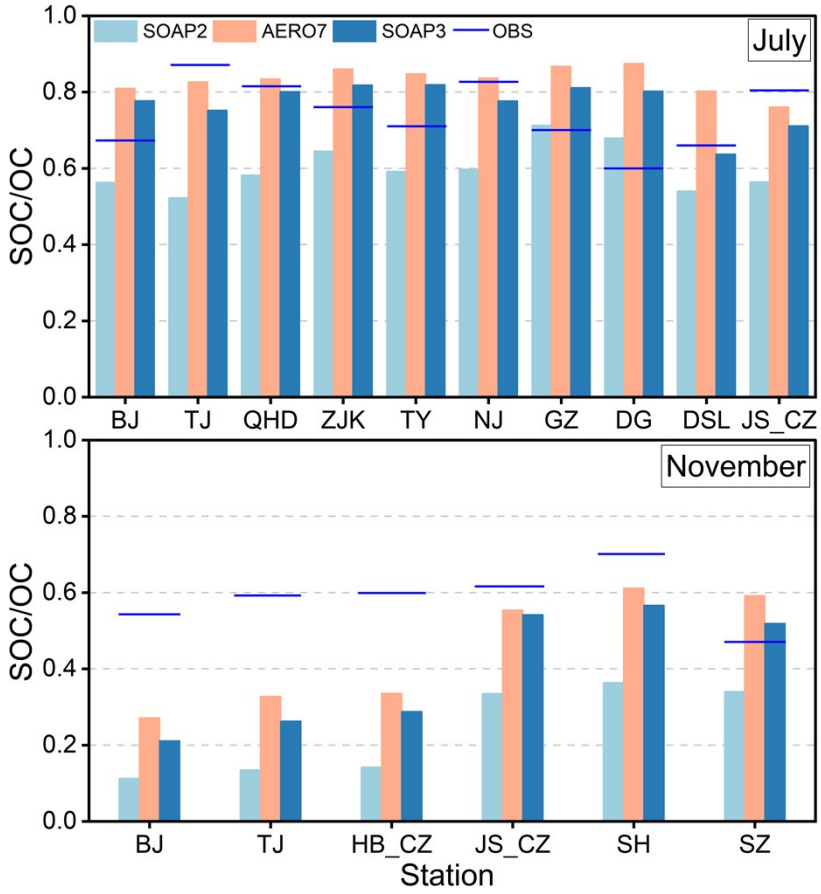

Figure S5 Monthly average observed and simulated SOC/OC for SOAP3 at 13 OC/EC observation sites in July and November 2018

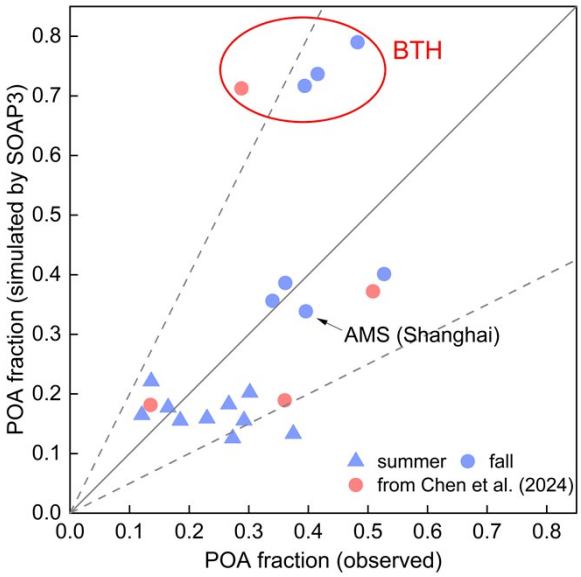

Figure S6 Comparison of observed and modeled POA fraction at various monitoring sites for different seasons (note that observation periods from Chen et al. (2024) do not perfectly align with the simulation period of this study).

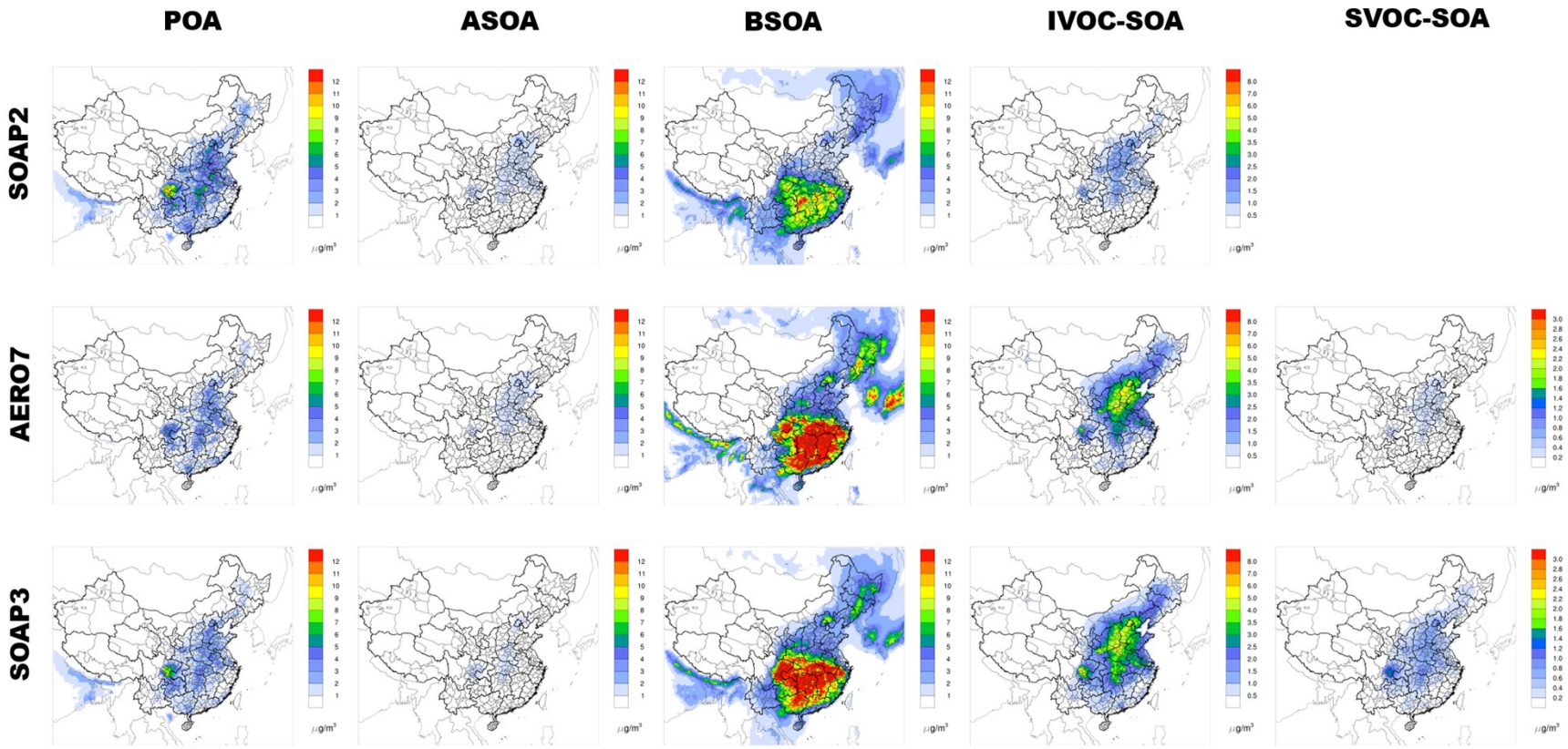

Figure S7 Spatial distributions of different OA components in July 2018

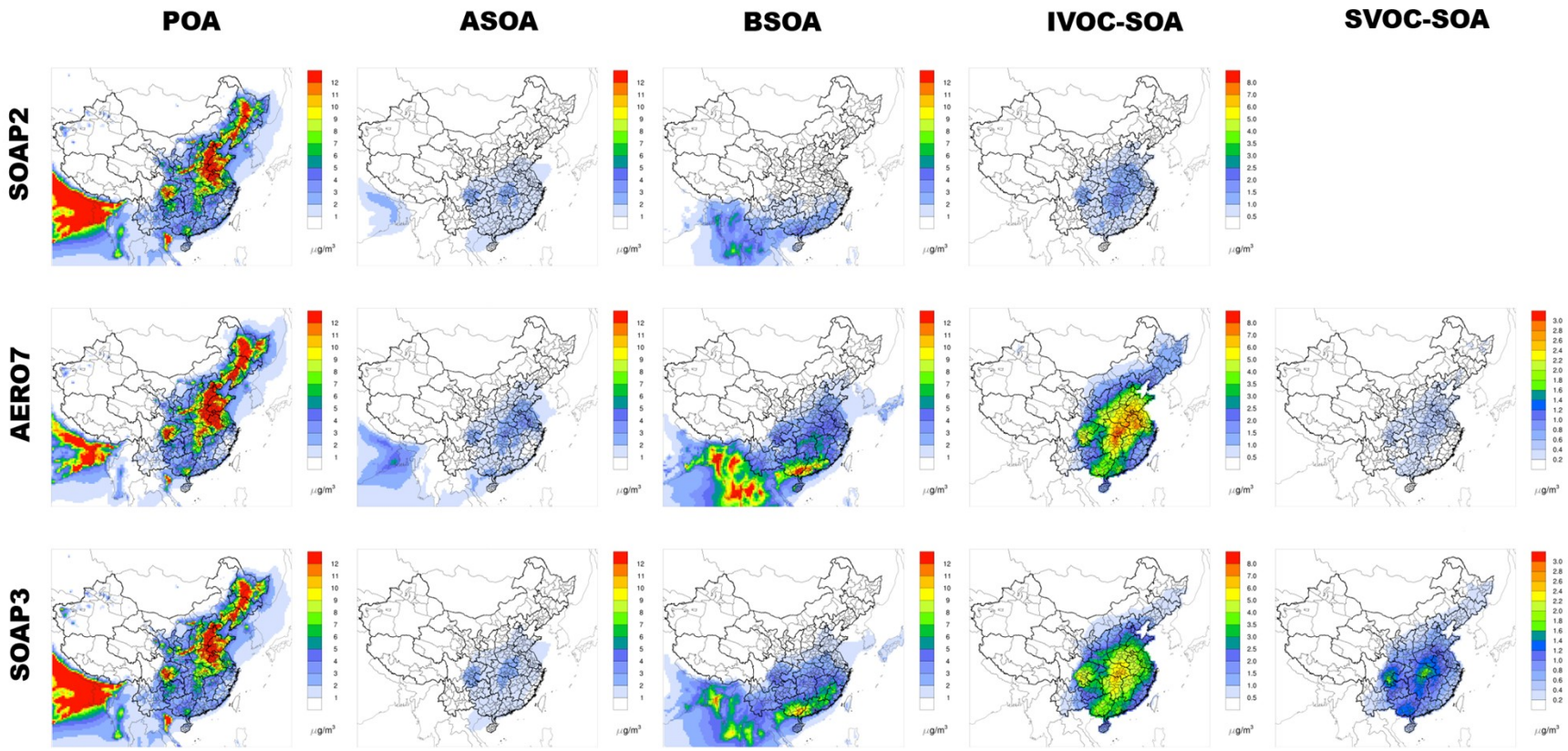

Figure S8 Spatial distributions of different OA components in November 2018

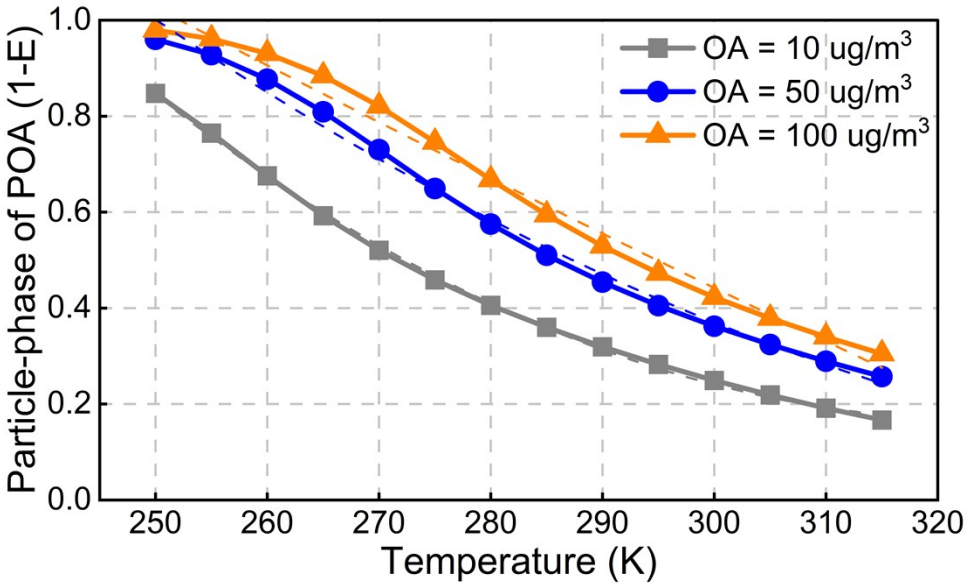

Figure S9 POA fraction in the particle phase as a function of temperature under different OA concentrations (10μg/m^3, 50μg/m^3, and 100μg/m^3)

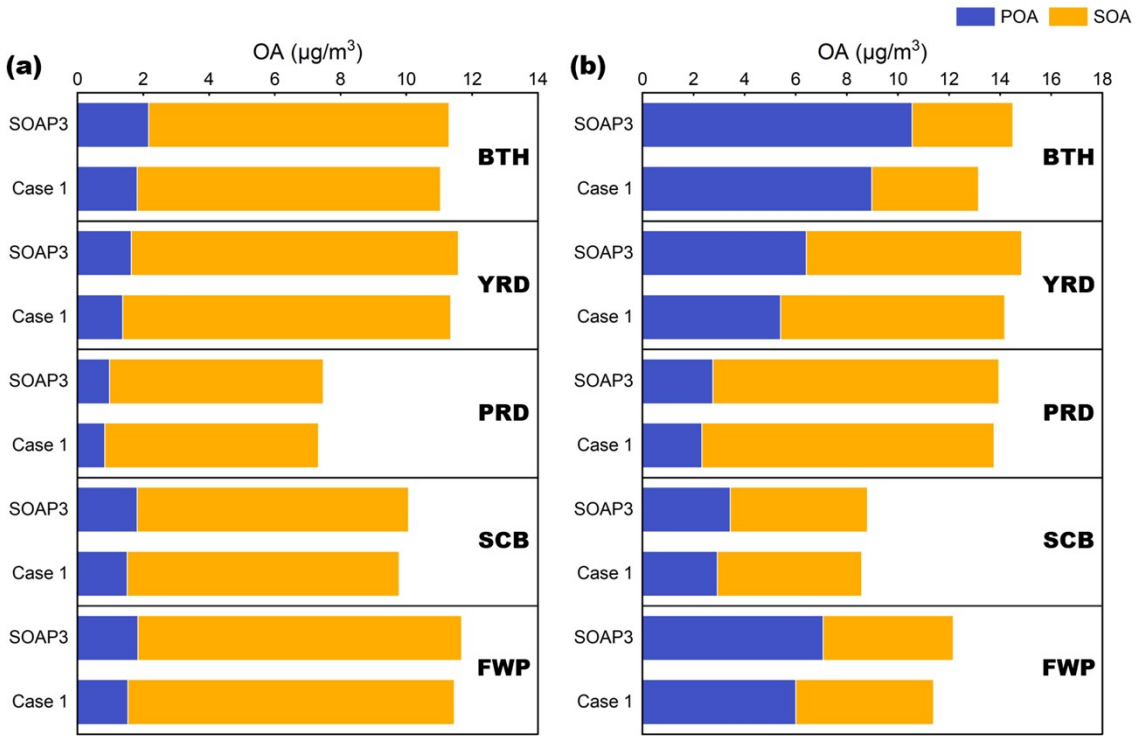

Figure S10 Comparison of simulated POA and SOA for (a) July and (b) November with different C_{OA} in deriving the temperature-dependent POA evaporation: Base (C_{OA} = 50 μg/m^3) and Case 1 (C_{OA}=20 μg/m^3)

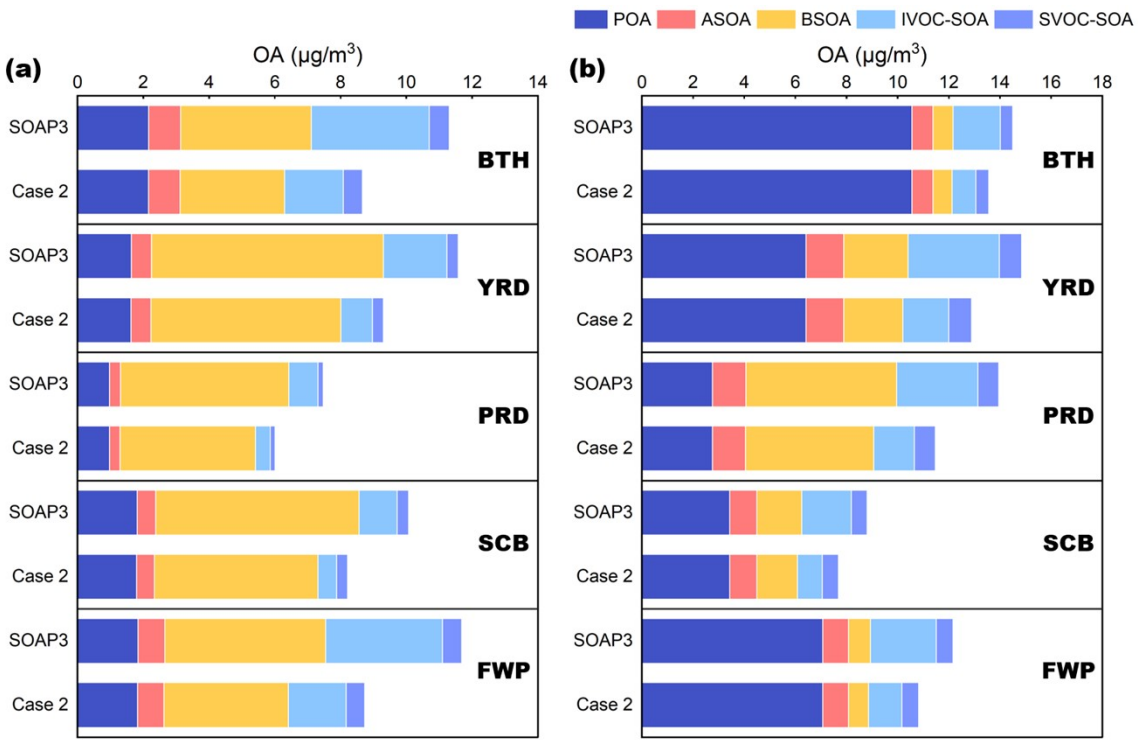

Figure S11 The impact of changing SOA yields from IVOC and BVOC on simulated OA components for (a) July and (b) November 2018. In Case 2, SOA yields from IVOC are reduced by 50%; SOA yields from BVOC under high-NO*x* conditions are set 30% lower than low-NO*x* conditions.

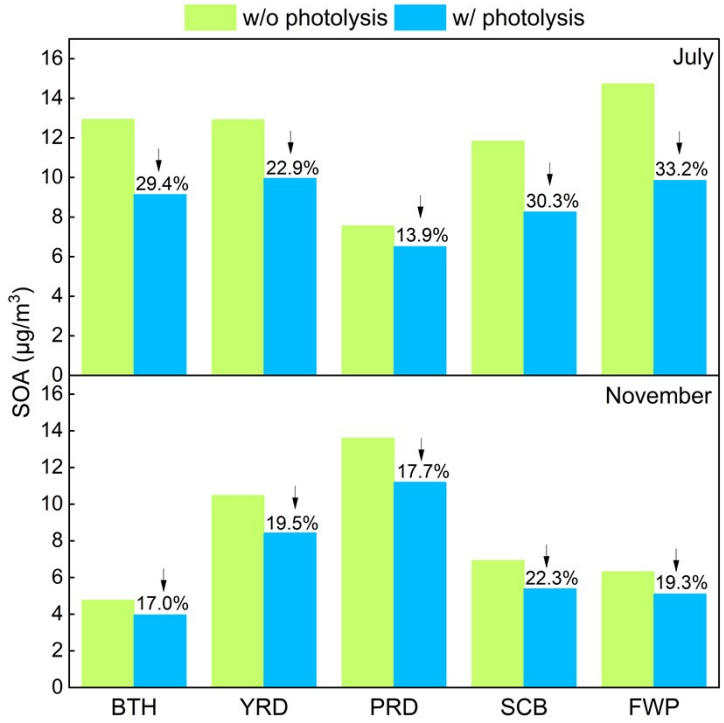

Figure S12 Effect of photolysis on SOA by the sensitivity simulation of the SOAP3 scheme

References

Huang, L., Liu, H., Yarwood, G., Wilson, G., Tao, J., Han, Z., Ji, D., Wang, Y., & Li, L. (2023). Modeling of secondary organic aerosols (SOA) based on two commonly used air quality models in China: Consistent S/IVOCs contribution but large differences in SOA aging. *Science of The Total Environment*, *903*, 166162. https://doi.org/10.1016/J.SCITOTENV.2023.166162

Walker, H., Stone, D., Ingham, T., Hackenberg, S., Cryer, D., Punjabi, S., Read, K., Lee, J., Whalley, L., Spracklen, D. V., Carpenter, L. J., Arnold, S. R., & Heard, D. E. (2022). Observations and modelling of glyoxal in the tropical Atlantic marine boundary layer. *Atmospheric Chemistry and Physics*, *22*(8), 5535–5557. https://doi.org/10.5194/ACP-22-5535-2022

Wu, L., Ling, Z., Liu, H., Shao, M., Lu, S., Wu, L., & Wang, X. (2021). A gridded emission inventory of semi-volatile and intermediate volatility organic compounds in China. *Science of The Total Environment*, *761*, 143295. https://doi.org/10.1016/J.SCITOTENV.2020.143295